Laboratory surface astrophysics experiment

Helen J. Fraser,[a] Mark P. Collings, and Martin R. S. McCoustra
School of Chemistry, University of Nottingham, University Park, Nottingham NG7 2RD, United Kingdom

(Received 29 October 2001; accepted for publication 22 February 2002)

In this article we describe the design and construction of a laboratory astrophysics experiment that recreates the harsh conditions of the Interstellar Medium (ISM) and is used to study the heterogeneous chemistry that occurs there. The Nottingham Surface Astrophysics Experiment is used to determine, empirically, accurately, and usually for the first time, key physical and chemical constants that are vital for modeling and understanding the ISM. It has been designed specifically to investigate gas–solid interactions under interstellar conditions. The pressure regime is ideally matched to molecular densities in dusty disks in protostellar or protoplanetary regions. The ultrahigh vacuum system is routinely capable of obtaining pressures that are only three orders of magnitude above those in the ISM, with similar relative concentrations of the two most abundant gases in such regions, H_2 and CO, and an absence of any other major gas components. A short introduction describes the astronomical motivation behind this experiment. In Sec. II we then give details of the design, construction, and calibration of each component of the experiment. The cryostat system has far exceeded design expectations, and reaches temperatures between 7 and 500 K. This is comparable with the ISM, where dust temperatures from 10 K have been observed. Line-of-sight mass spectrometry, reflection absorption infrared spectroscopy, and quartz crystal microbalance mass measurements were combined into a single instrument for the first time. The instrument was carefully calibrated, and its control and data acquisition system was developed to ensure that experimental parameters are recorded as accurately as possible. In Sec. III we present some of the experimental results from this system that have not been published elsewhere. The results presented here demonstrate that the system can be used to determine desorption enthalpies, $\Delta_{des}H$, bonding systems, and sticking probabilities between a variety of gases and ices common to the ISM. This instrument will greatly facilitate our understanding of surface processes that occur in the ISM, and allow us to investigate ''mimic'' ISM systems in a controlled environment. In this article we illustrate that laboratory surface astrophysics is an exciting and emerging area of research, and this instrument in particular will have a major impact through its contributions to both surface science and astronomy. [DOI: 10.1063/1.1470232]

I. INTRODUCTION

Molecular astrophysics has developed rapidly over the last 25 years, and it is widely recognized that an understanding of the chemical processes that occur in the vast regions of space between stars [Interstellar Medium (ISM)] will provide a gateway to understanding key aspects of star and planetary formation[1] and, possibly, to the origins of life itself.[2] The main processes by which interstellar molecules are formed and destroyed in the gas phase are now reasonably well understood, but gas-phase chemistry alone is unable to successfully account for the variety and richness of molecular species in the ISM. The presence of dust in the ISM was first inferred from the reddening and polarization of background starlight. More recently, the Infrared Space Observatory (ISO) has provided a wealth of evidence that ice is deposited on dust grains in the giant gas clouds in the dense ISM. It is now recognized that physical and chemical processes that occur at the surfaces of interstellar grains are crucially important, e.g., atomic and molecular adsorption/desorption at grain surfaces,[3] surface-catalyzed chemical reactions,[4] and energetic surface processing [by cosmic rays and ultraviolet (UV) radiation].[2]

An ISM dust grain is thought to consist of a silicate or carbonaceous core surrounded by a ''bulky'' molecular ice layer, typically 20 nm in diameter (see Fig. 1). Ices are accreted either by adsorption (freeze out) from the gas phase or from reactions between accreted atomic, radical or molecular species on the grain surface. A number of molecular species have been detected in the ISM that could only have been formed through surface reactions, e.g., CH_3OH, SO_2,[5] the energy barrier in the gas phase precluding the reaction from ever occurring. Furthermore, the relative abundance of the simplest and most common molecule in the universe, H_2, cannot be fully explained unless surface reactions are included in chemical models of our universe. Very little is currently understood about the prevailing physical conditions: observational astronomers are able to provide us with snapshots of different regions of the ISM at various stages of development, from the diffuse ISM to dense molecular clouds. Understanding the chemical evolution of such re-

[a]Author to whom correspondence should be addressed; current address: Raymond and Beverly Sackler Laboratory for Astrophysics, Leiden Observatory, University of Leiden, Postbus 9513, 2300 RA Leiden, The Netherlands; electronic mail: fraser@strw.leidenuniv.nl

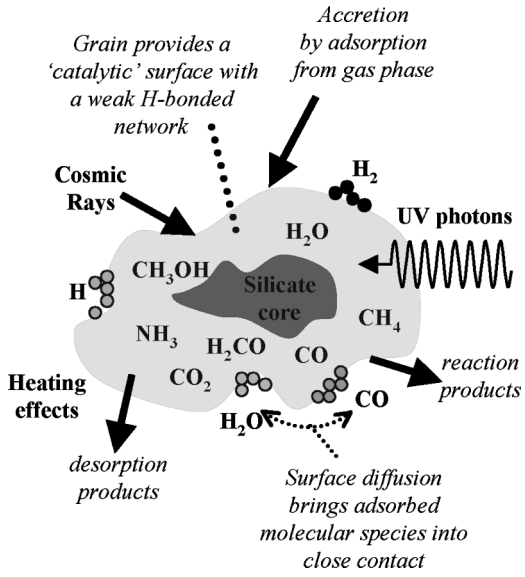

FIG. 1. Illustration of the make up of an icy dust grain in the ISM and the typical energetic processes to which it is exposed.

gions provides us with a major route by which to link all the observations together. In addition, these regions eventually collapse under their own gravitational field and form protostellar objects, the precursors to new stars, planets, and solar systems. Because this collapse occurs on approximately the same time scale as the chemical evolution, it is thought that chemistry is one of the key driving forces behind the onset of new star formation.[6]

The provision of data is key to this linking process, specifically, accurate empirical data pertaining to sublimation rates, binding energies, and sticking probabilities of all the major molecular and atomic species on astronomically relevant surfaces. It is also necessary to identify the key surface chemical reactions that occur in the ISM, and the energy barriers, reaction rates, kinetic schemes, and (in cases where multiple products are formed) branching ratios of such reactions. In most modern astrophysical models, molecular constants from gas-phase experiments are employed, these being the only data available. This leads to a gross misrepresentation of the chemical evolution, with certain key reactions that may only occur at surfaces being ignored, and overrepresentation of the production and abundance of other chemical species. Laboratory surface astrophysics also provides qualitative information on the physical and chemical effects that astrophysical processes have on accreted ices. In particular, the thermal processing of accreted ices is a key evolutionary indicator in the ISM that provides information on the energetic history of the ice mantles during star birth and protostellar evolution.

The Nottingham Surface Astrophysics Experiment (NoSAE) was designed and constructed to address these issues. Operating at ultrahigh vacuum (UHV) pressures and cryogenic temperatures, the experiment mimics the harsh conditions found in ISM regions in a controlled environment. The system reaches temperatures of 10–500 K, similar to temperatures in ISM, protostellar, and circumstellar disk environments. The base pressure is better than 2×10^{-10} mbar, only a few orders of magnitude higher than the typical pressure in the dense interstellar medium, and a few orders of magnitude lower than the base pressure in dusty protostellar and circumstellar disks. Furthermore, the experimental vacuum is dominated by H_2, just like the ISM. The chamber is equipped with a number of traditional surface science instruments, including a Fourier transform reflection–absorption infrared spectrometer (FT-RAIRS), a quartz crystal microbalance (QCM), and a quadrupole mass spectrometer (QMS). These instruments are used to obtain quantitative spectroscopic data and qualitative measurements of binding energies and sticking probabilities in astrophysically relevant surface-adsorbate systems.

In this article we describe the NoSAE apparatus in detail, highlighting those elements of the experiment that digress from standard UHV surface science instrumentation. To demonstrate the experiment's capabilities, preliminary results from several molecular-ice systems are presented. It is envisaged that this surface astrophysics experiment will contribute to our fundamental understanding of gas–solid processes that occur in the ISM. The experiment will generate essential basic data for astrophysics as well as stimulating new and innovative work in surface physics and chemistry, particularly studies of low temperature molecular solids.

II. EXPERIMENTAL DESIGN

A. Overview

A schematic of the NoSAE is shown in Fig. 2. The apparatus comprises a 30 cm diameter, cylindrical, stainless-steel chamber (Instrument Technology Ltd.), pumped by a liquid N_2 trapped, 9 in. oil diffusion pump (Edwards High Vacuum Ltd.), and a titanium sublimation pump (Instrument Technology Ltd.), backed by a mechanical rotary pump (Edwards High Vacuum Ltd.). Access ports (directed toward the center of the chamber) are provided at four levels on the main chamber, as well as at the top and base, for sample mounting, effusive gas dosing of substrates and adsorbates, surface analysis, and system monitoring. A base pressure of better than 2×10^{-10} mbar is routinely achieved after baking at 120 °C for between 48 and 72 h. The chamber is equipped with a differentially pumped, precision $XYZ\theta$ manipulator (Caburn–MDC Ltd.) that supports an UHV compatible closed-cycle helium cryostat (APD Cryogenics) that is capable of reaching temperatures below 10 K. The substrate is a gold-coated quartz crystal, which is one half of a heterogeneous QCM, designed specifically for this experiment and capable of working at cryogenic temperatures (Oxford Applied Research Ltd.). Molecular ices are grown *in situ* by direct vapor deposition from the gas phase. Gases are mixed on a dedicated gas handling line, and then introduced into the chamber via a pair of fine control leak valves (VG Ltd.). The mass of the deposited film can be measured directly using the QCM. The chamber is also equipped with two differentially pumped infrared (IR) windows for surface analysis by FT-RAIRS (BioRad). A dedicated temperature control system and a line-of-sight configured quadrupole mass spectrometer (Hiden Analytical Ltd.) are fitted for temperature programmed desorption (TPD) measurements. A hot-cathode

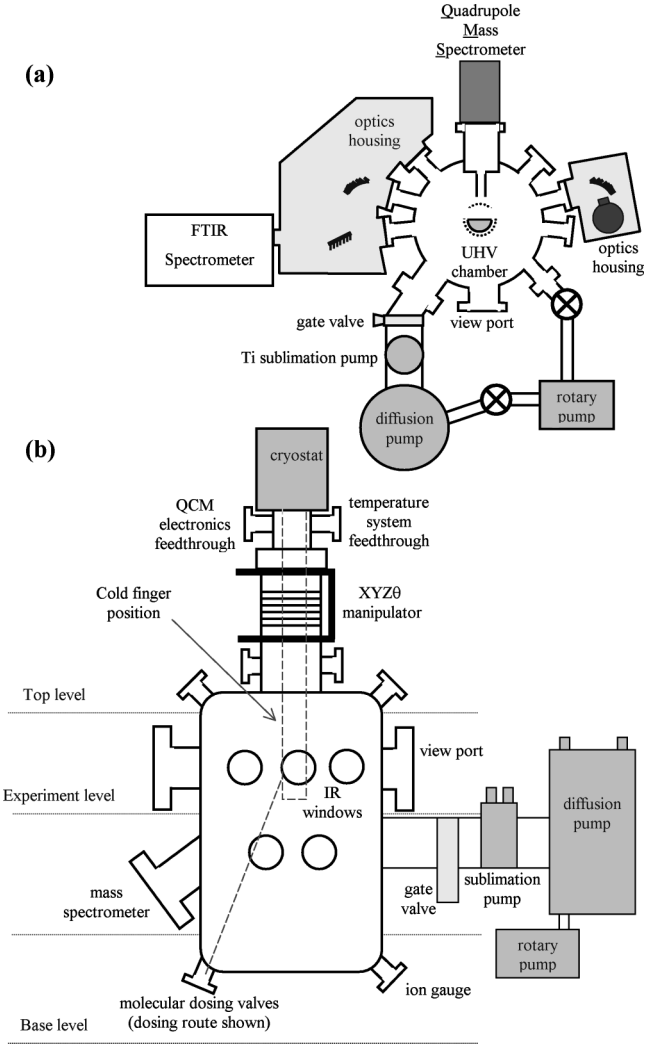

FIG. 2. Schematic of the NoSAE from the (a) top and (b) side.

ion gauge (Edwards High Vacuum Ltd.) and viewing port are also fitted to the chamber for monitoring purposes.

B. Quartz crystal microbalance

Quartz crystal microbalances are routinely employed for thin-film thickness monitoring, chemical sensing, and mass measurements at room temperature.[7] In a QCM, mass is monitored at the surface of an oscillating quartz crystal. Minute changes in the crystal's surface mass, Δm, result in pronounced shifts, Δf, in the crystal's resonant frequency, f_0, described by the Sauerbrey equation,[8]

$$\Delta f = -\frac{2 f_0^2 n}{A\sqrt{\mu\rho}}\Delta m, \tag{1}$$

where n is the harmonic index of the resonant frequency, A is the exposed surface area of the crystal, μ is the shear modulus of quartz (2.947×10^{11} g cm^{-1} s^{-2}), and ρ is the density of quartz (2.648 g cm^{-3}). The QCM in this system was designed specifically to operate under UHV and cryogenic conditions. It was custom developed for this experiment (from a standard QCM) by Oxford Applied Research, and further modified by the Electronics Department in the School of

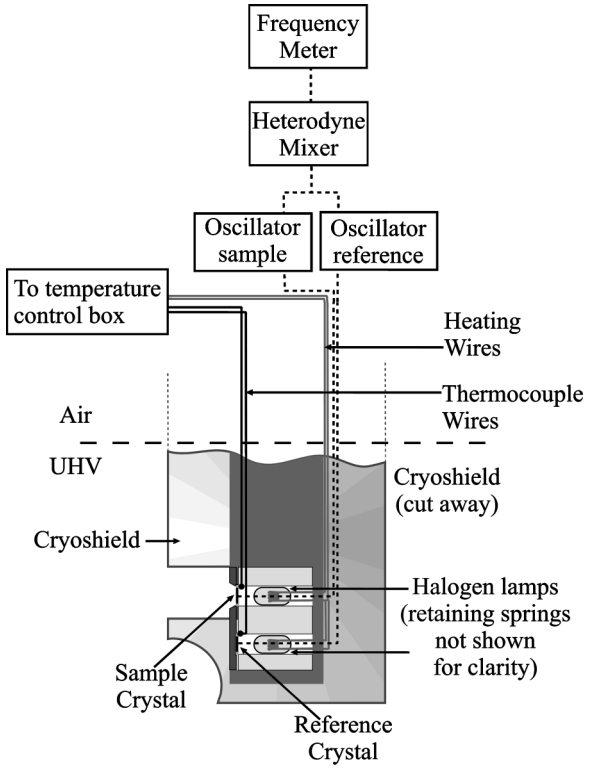

FIG. 3. Schematic of the arrangement of the QCM system in the NoSAE experiment.

Chemistry, University of Nottingham. A schematic of the system is shown in Fig. 3.

Two, 8 mm diameter AT-cut quartz crystals, with resonant frequencies of around 15 MHz, are mounted in close proximity to each other. The crystals are incorporated into a standard Colpitt oscillator circuit, using discrete components, and the capacitance tolerances across the crystals are determined by *in situ* testing. To achieve UHV, it is necessary to bake the whole system, including the QCM, to 120 °C. Consequently, unlike conventional QCM systems, all the electronics for the QCM system are mounted outside the UHV chamber, and the total cable length between the quartz crystals and the oscillator circuits is around 2.5 m! Braided, Kapton inner-coated coaxial cables are enclosed in bakable sheathing, and are wound around the cryostat's cold finger to ensure that they do not present an additional heat load at the cryostat's cold tip. One crystal is exposed to the UHV vacuum chamber (the sample crystal), the other is screened by a gold-coated oxygen-free high-conductivity (OFHC) copper plate (the reference crystal). Two different front plate designs are utilized in the experiment. The first, a single plate with a small access hole directly above the sample crystal, is used for line-of sight TPD and thin-film deposition measurements. With this plate, RAIR spectra are measured directly from the gold-plated surface above the reference crystal. The second plate is split into two pieces and is used to measure RAIR spectra and TPD measurements directly from one of the quartz crystals. However no QCM mass deposition measurements are made in this mode since the long-term stability of the QCM signal is affected by the reduction in contact area between the crystal and the front plate. The signal from the sample crystal is heterodyned with that from the refer-

ence crystal in a standard IFGET mixer circuit: the difference frequency is directly related to the mass of material deposited on the sample crystal. This frequency difference will typically be much less than 1% of the resonant frequency of the individual crystals, thereby allowing very small changes in the frequency (and therefore mass) to be detected. The heterodyne difference frequency is amplified to 1 V peak to peak, and rectified to produce a sharp-edged square-wave signal. The signal is fed into a SR620 timer counter (Stanford Research Systems Ltd.), where the frequency is derived with a 0.1 s gate time, over a sample size of 200 cycles. The output signal is recorded to a PC via a general purpose interface bus (GPIB) (see Sec. II F). The system's sensitivity is 1.02×10^{-9} g Hz^{-1}.

A quartz halogen bulb (Welch Allen, 14 V, 179 A) is spring mounted behind each quartz crystal. This allows each crystal to be individually heated to around 200 °C for flash cleaning, and can also be used to heat the crystals from cryogenic temperatures. An *E*-type thermocouple is sandwiched between each crystal and the front plate. Further specific details of the temperature control system are given in Sec. II C. Clearly, over the temperature range of this experiment (10–520 K) the change in the crystal's resonant frequency with temperature is significantly greater than the change in frequency due to mass. The QCM housing is constructed of gold-plated OFHC copper, and is designed to act as a temperature stabilized oven/chiller. The housing is mounted onto the cryostat's cold finger via a M6 double screw thread: thermal contact between the housing and the cryostat is maximized by using ultrathin (<10 μm) AG foil washers. During moderate warming or cooling (<1 K s^{-1}), the temperature gradient across the two QCM crystals is minimized to less than 1 K, and each crystal exhibits approximately the same frequency response with the temperature. In practice, the QCM heterodyne signal has a small negative slope during cooling and a similar, positive slope during heating, primarily due to the different thermal response, stress, and relative acoustic impedance of each crystal in its individual environment.

C. Temperature control system

The temperature control system on this apparatus was designed in collaboration with the Electronics Workshop in the School of Chemistry, University of Nottingham, such that experimental data could be recorded over a range of temperatures that are significant in the ISM. This system is capable of measuring temperatures between $\approx$7 and 500 K and heating rates between 0.01 and 0.1 K s^{-1}.

Cryogenic temperatures are reached using a commercially available, closed-cycle helium cryostat (Displex 202, APD Cryogenics Ltd.). The QCM sample stage, described above, is mounted at the base of a 1 m OFHC copper cold finger that is welded to the cryostat expander unit. A Ni-plated, OFHC copper radiation shield is also attached to the helium return line on the expander unit, and it completely encloses the cold finger and the sample, except for a 1 cm wide slit in the main body and a 1 cm diameter hole in the base that allows experimental access to the substrate. The whole system can be cooled from room temperature to <10 K in around 4 h. The sample can be heated either by radiation from the two halogen bulbs located inside the QCM housing (Welch Allen, 14 V, 1.79 A), or by a 50 W resistive heater at the end of the cold finger, or both. To increase the lifetimes of the bulbs, their maximum voltage is limited to 10 V. An *E*-type thermocouple (Chromel–Constantan) is attached between the sample's front plate and each of the QCM crystals: A *KP*-type thermocouple (0.7% Fe in Au–Chromel) is attached to the base of the cold finger. All the electrical and thermocouple wires are wound tightly along the entire length of the cold finger to minimize the conductive heat load to the cold end. *E*-type thermocouples have relatively high thermovoltages at cryogenic temperatures, low thermal conductivity, and can measure temperatures to beyond 500 K. Below 25 K however, their response is decidedly nonlinear. *KP*-type thermocouples are at least three times more sensitive than *E*-type thermocouples over cryogenic temperatures (up to around 150 K), and show greater linearity in their V–T curve characteristics, but are much less sensitive than the *E*-type thermocouples above room temperature. The wires are spot welded to a 10-pin ceramic and copper feedthrough at the top of the UHV system [see Fig. 2(b)]. The thermocouple voltages are referenced against a temperature-stabilized reference oven at 352.7 K, amplified, and fed via a 14-bit data acquisition board (DAQ) into a PC (see Sec. II F for more details). For improved accuracy over the temperature ranges of interest, three temperature scales (amplification circuits) are used, 0–100, 90–210, and 0–500 K. In each case 0 V output from the measurement box corresponds to the lower limit, and 10 V output to the upper limit. Details of the system electronics may be obtained from the authors if required. Two digital set-point controllers (Omron Corporation, E5CK), are also linked to the PC via RS232 links. Each controller box is linked to one of the *E*-type thermocouples and the corresponding halogen bulb behind the QCM crystals. In an isothermal experiment, the set point required is input to the control box, which then uses the thermocouple voltage as a feedback system to establish the exact bulb current that is required to maintain the set-point temperature. A small degree of hysteresis is evident close to the setpoint but, once damped, the controllers can maintain the substrate temperatures to better than 0.1 K. When heating ramps are required the setpoint is generally fixed far beyond the required endpoint of the experiment to ensure a linear heating ramp is obtained. The heating rate can be adjusted by additional heating from the cryostat tip heater, changing the maximum voltage across the halogen bulbs, or using different set-point voltages and ramp time settings on the controllers. With this method, it is possible to obtain linear heating ramps between 0.1 and 0.01 K s^{-1}.

It was necessary to calibrate the measurement system over each range: first, to enable these amplified voltages to be reconverted into temperatures; second, to provide an accurate estimate of the ultimate substrate temperature; and third, to account for deviations between the theoretical and experimental values of the thermocouple output voltages that arise from different wire samples, amplifier circuits, drift, and vacuum effects. The calibration involved cooling the

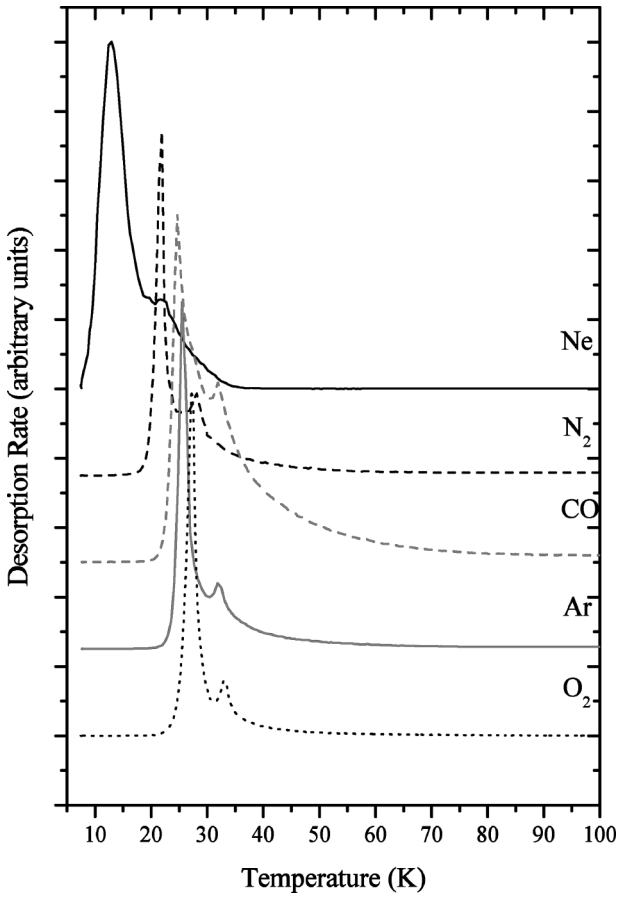

FIG. 4. TPD spectra of Ne, N_2, Ar, CO, and O_2 on Au used for the temperature calibration. Each desorption profile shows both multilayer and monolayer desorption peaks, with the monolayer desorption peak appearing on the high temperature side of the multilayer peak in each case.

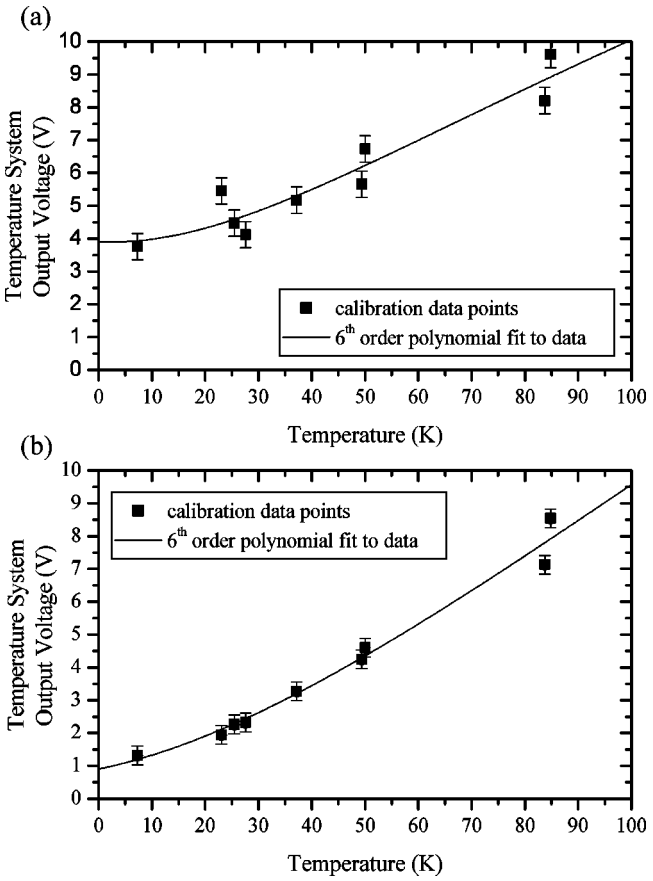

FIG. 5. Experimentally derived $V-T$ calibration curves for (a) *E*-type and (b) *KP*-type thermocouples on the 0–100 K range.

crystal to its base temperature, depositing multilayers of gas on the substrate, and then recording the TPD spectrum as the substrate was warmed.[9,10] Assuming that lateral interactions between the adsorbate molecules are negligible, the pressure and thermocouple voltage at the maximum in the TPD multilayer desorption curve correspond to the point at which the gas desorption flux is in equilibrium with the flux expected from a gas at the same temperature and with a vapor pressure equal to that of the solid. To first approximation this ''sublimation'' temperature, T_s, can be calculated directly from the Clausius–Clapeyron equation,[11]

$$T_s = \frac{1}{[(1/T^*) - (R/\Delta_{\mathrm{sub}}H)\ln(P_s/P^*)]}, \tag{2}$$

where T^* is the boiling point (K) at atmospheric pressure, P^* is atmospheric pressure (101 325 Pa), R is the gas constant (8.314 510 $\mathrm{J\,K^{-1}\,mol^{-1}}$), P_s is the partial pressure of the desorbing gas in the UHV system at the TPD maximum, and $\Delta_{\mathrm{sub}}H$ is the enthalpy of sublimation ($\mathrm{J\,mol^{-1}}$), given by

$$\Delta_{\mathrm{sub}}H = \Delta_{\mathrm{vap}}H + \Delta_{\mathrm{melt}}H, \tag{3}$$

where $\Delta_{\mathrm{vap}}H$ is the enthalpy of vaporization and $\Delta_{\mathrm{melt}}H$ is the enthalpy of melting (both in $\mathrm{J\,mol^{-1}}$). TPD spectra were measured for Ar, CO, CO_2, CH_4, H_2, Kr, N_2, Ne, and Xe (see Fig. 4). The TPD spectra of these simple species have been reported extensively from a variety of well defined surfaces, e.g., those reported in Refs, 9 and 12–21, and are used in this case solely for calibration purposes. Therefore the values of T_s calculated from Eq. (2) were plotted against the thermocouple voltage readings for each gas, and fitted to a sixth order polynomial curve using a nonlinear least-squares fitting routine. The curves describe the $V-T$ characteristics of each thermocouple in the system over a particular temperature scale (Fig. 5 shows $V-T$ curves in the 0–100 K range). For the *E*-type thermocouple, changes in crystal temperature can be measured to ≈0.5 K on the high-resolution scales and to ≈0.8 K on the full-range scale. For the *KP*-type thermocouple, changes in crystal temperature can be measured to ≈0.1 K on the high-resolution scales and to ≈0.5 K on the full-range scale. Furthermore, the formation of both H_2 and Ne multilayers on the substrate is evidence that the ultimate substrate surface temperature is below 6 K.

D. Line-of-sight mass spectrometer

The design of the line-of-sight mass spectrometer (LoSMS) is based on a design by Jones and Turton for line-of-sight sticking probability and TPD measurements.[22] These methods have been described in detail by Jones and Turton, but a brief description is given here to explain the motivation behind the LoSMS design. In LoS TPD, the mass spectrometer is mounted in a liquid N_2 cooled shroud, with two small apertures defining the direct path between the surface and the

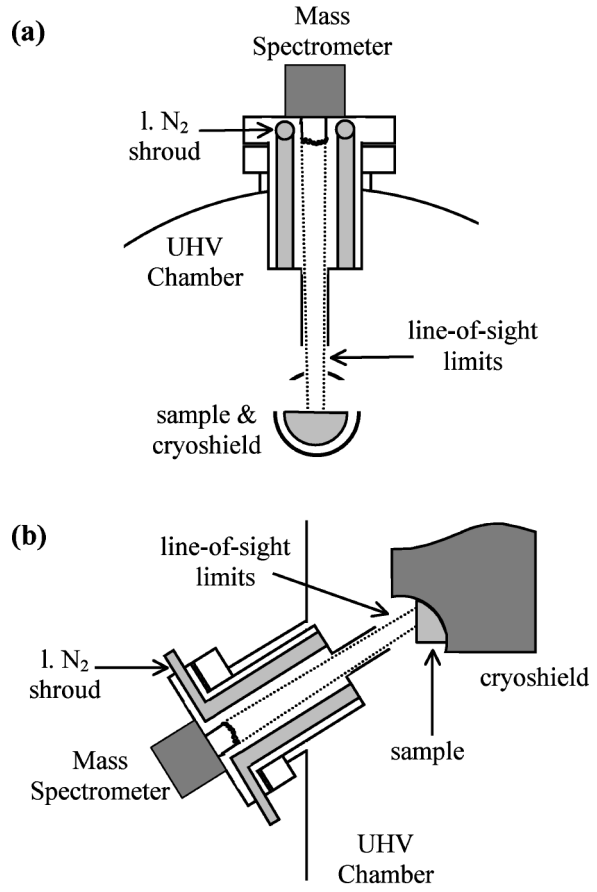

FIG. 6. Depiction of the LoSMS arrangement in the NoSAE experiment (a) from above and (b) from the side. The maximum molecular trajectory limit is indicated by the dotted lines between the surface and the ionization region in each case.

ionization region. Consequently, only those molecules that desorb from a small, well-defined patch on the substrate, which can then reach the ionization region of the mass spectrometer by direct flight, are detected. The mass spectrometer detector element is ''blind'' to all molecules that emanate from outside the LoS area of the substrate, since their trajectories lead to collisions with the shroud wall where the molecules condense out to a low vapor-pressure solid. Liquid N_2 cooling is sufficient to trap almost all astronomically relevant molecular species, with the exception of H_2, CO, and N_2, and the noble gases, He, Ar, Ne, and Kr. In LoS sticking probability measurements, the UHV chamber is backfilled to a specific gas pressure, and the sample is moved out of the mass spectrometer's LoS. In this configuration the mass spectrometer signal originates from the chamber wall opposite the aperture, and is directly proportional to the total gas pressure in the chamber, provided that the sticking probability of the gas on the chamber walls is zero. The sample is then moved into position in front of the mass spectrometer, and the flux from the sample surface can be measured directly. If a correction is made for the difference in temperature between the sample and the gas, the sticking probability can then be calculated, independent of both the system's pressure gauge response and surface coverage calibrations.

Figure 6 shows a top and a side view of the LoSMS arrangement in this experiment. The mass spectrometer is a commercially available, UHV compatible, quadrupole mass spectrometer with an ion-counting secondary electron multiplier (SEM) detector from Hiden Analytical Ltd. (HAL-RC 3F-PIC). It is mounted in a custom built liquid N_2 shroud, which extends the full length of the mass spectrometer's quadrupoles and ionization chamber. The mass spectrometer is capable of reading partial pressures to 5×10^{-13} mbar at mass resolution of 0.1 m/e. The ionization region is connected directly to the main chamber's diffusion pump, and is also equipped with a titanium sublimation pump (Instrument Technology Ltd.) to allow differential pumping and to reduce contamination. The LoS between the sample and the detector is defined by a narrow, OFHC copper tube, 150 mm long, mounted at the end of the liquid N_2 shroud. A small hole at the base of the cryostat cold shield acts as a third aperture between the mass spectrometer and the sample: the shield temperature is typically 30–35 K, so desorption from the shield can be ignored.

Initially, the mass spectrometer was calibrated against the ion gauge using N_2. Specific mixed gas ratios were then used to obtain ion counts s^{-1} to partial pressure conversion factors, and ionization efficiencies (relative to N_2) for the most commonly used system gases. Cracking fraction patterns and conversion factors for the cracking fractions were also measured. For small species, such as He, the conversion factors were around 6×10^{-13} mbar counts s^{-1}; for larger species, such as H_2O this figure was around 2×10^{-12}; for heavy species the conversion factors were around 3×10^{-11}. The calibrated mass spectrometer signals were used, in turn, to calibrate gas flow rates into the chamber at specific leak valve settings. The leak rates are reproducible within a few percent, although some hysteresis exists between the clockwise and anticlockwise motion of the valves. These data are clearly useful in estimating dosing times and pressures to obtain specific ice thicknesses, measuring uptake curves, measuring sticking probabilities where LoS methods are inapplicable, setting multiple ion detection scans for TPD measurements, and calculating surface coverages from TPD spectra. However, such calibration data are clearly system specific, and are therefore not reproduced here.

E. FT-RAIRS

FT-RAIRS is an established, nondestructive surface science technique which probes vibrational modes of species adsorbed on surfaces. The technique is described in detail elsewhere.[23,24] Its major advantage over transmission infrared spectroscopy is that it can be used to detect intra-adsorbate and adsorbate–substrate vibrations and adsorbate–adsorbate interactions at monolayer and submonolayer coverages on metal surfaces, provided that a component of their dipole moment transition lies perpendicular to the surface. Greenler quantitatively calculated the absorption intensity as a function of incidence angle and found that, for an adsorbate on a metal surface, the signal reaches a maximum at grazing incident angles (85°–88°).[25] This experiment is equipped to use RAIRS at incident angles of 85.5°, 84°, 75°, 70.5°, 60°, and 45°.

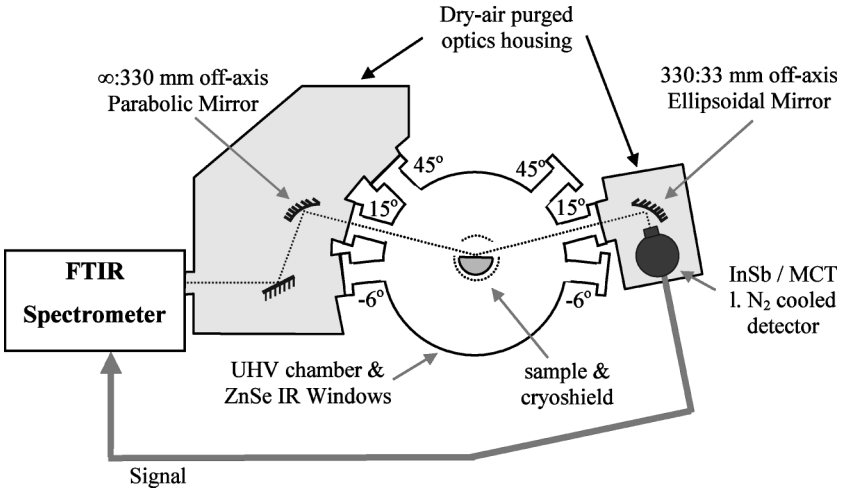

FIG. 7. Bird's-eye view of the FT-RAIRS system.

A top view of the RAIRS system is shown in Fig. 7. A BioRad FTS-40A FTIR spectrometer is used, which contains an IR source and a 60° interferometer. The external beam from the spectrometer is steered using one or two planar mirrors (depending on the incidence angle at the substrate) and focused onto the substrate. The focusing mirror is a custom-made 90° off-axis parabolic mirror (∞: 330 mm), with a 195 mm primary focal length. It was custom manufactured from heat-treated Al by Aero Research Associates Inc., and the parabolic face is 50 mm in diameter, polished to 150 Å. The beam waist is focused to 5 mm at the center of the chamber. The Au coating on the sample crystal or QCM front plate acts as a reflective mirror. The beam is focused onto the detector element [a 2 mm diameter, liquid N_2 cooled, InSb detector operating in a photovoltaic (unbiased) configuration (BioRad), or a 2 mm diameter, liquid N_2 cooled, mercury–cadmium–telluride (MCT) detector operating in a photocurrent configuration (BioRad)]. The focusing mirror is a custom-made (Aero Research Associates Inc.), 90° off-axis ellipsoidal mirror (10:1 ratio), with a 181.5 mm semi-major axis, and a 165 mm semi-minor axis. It is also manufactured from heat-treated Al, and to the same dimensions and tolerances a the parabolic mirror. The output signal from the detector is amplified and fed back into the data acquisition PC via the BioRad FTIR spectrometer. Generic BioRad software is used to process the final FT-RAIR spectrum.

The entire optics are housed in dry-air/N_2 purged enclosures. The lids of the enclosures can be removed for alignment purposes. Rubber seals are placed between the FTIR spectrometer (also purged), lids, chamber connectors, and enclosures. A slight overpressure purge removes gas contaminants from the IR beam path, and improves the quality of the FT-RAIRS spectra measured. During bakeout the enclosures are removed from the system.

The UHV chamber and purged IR-optics enclosures are separated from each other by differentially pumped KBr windows that were designed specifically for this experiment (Instrument Technology Ltd.). The optics enclosures can be moved onto symmetric ports, fixed onto the UHV chamber at angles of 84°, 75°, and 45° (as shown in Fig. 7) to conduct RAIRS at 84°, 75°, and 45°, or they can be fixed at asymmetric ports, and the sample itself can be rotated to accommodate RAIRS at 85.5°, 70.5°, and 60°. These changes in angle can be accommodated without breaking the UHV conditions. The KBr windows are mounted on a Viton O ring in a shallow recess of a CF40 flange, and are secured from the atmospheric side by a threaded retaining ring. The flange itself is attached to the UHV chamber with a Cu gasket. The optics enclosures fit tightly over the outer edge of these flanges. Even when the enclosures are overpressured, the UHV vacuum can be maintained at better than 2×10^{-10} mbar.

F. Data control and acquisition system

Control and data acquisition for the NoSAE experiment is maintained from two, network-linked, IBM compatible PCs. An overview of the system is given in Fig. 8. Manufacturers' generic software are used to control the BioRad FTIR spectrometer (via a generic communication card and link) and the Hiden quadrupole mass spectrometer (via a RS232 serial link). All other instruments are controlled by a data acquisition program written specifically for this purpose us-

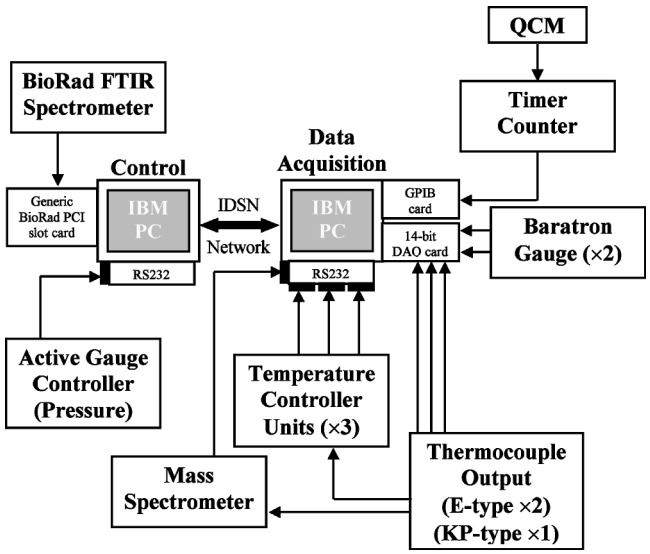

FIG. 8. Salient features of the NoSAE data control and acquisition system.

ing HP-VEE.[26] It records frequency data from the timer counter in the QCM system via a GPIB interface: pressure data from the UHV system via a serial link from an Edwards active gauge controller (Edwards High Vacuum Ltd.) and temperature data from the temperature control system via a 14-bit DAQ interface. The voltage output from the temperature control system is also read into an auxiliary input on the mass spectrometer; in TPD experiments this auxiliary channel is monitored concurrently with the mass data, and no further processing is necessary to obtain the TPD spectrum directly. All three software programs output tab separated ASCII data files that can be read into a single spreadsheet for analysis.

III. APPLICATIONS

A. TPD

Temperature programmed desorption is a common technique employed in surface science which is described extensively elsewhere.[27] Briefly, the surface under investigation is exposed to one or more adsorbate gases in varying surface concentrations. The surface is then heated, using a linear heating ramp, and a mass spectrometer is used to monitor the desorption rate of both the reagents and any reaction products against temperature. This technique has been widely employed to study surface catalysis on well-defined single crystal surfaces and desorption of thin molecular films,[27] e.g., for molecular solids such as CO, O_2, Ar, and N_2.[9,12–21] There have also been a number of coadsorption studies at low temperature.[28] However, very few UHV surface science experiments are capable of operating below 10 K, and almost no TPD data exist on desorption of multilayer thin films consisting of molecular mixtures coadsorbed below 10 K. These data pertain directly to the situation in the ISM and, as we show in this article, the results of these experiments give very different results from studies in which higher temperature (i.e., 20–80 K) deposition of only one molecular species is undertaken.

The preliminary TPD results from this experiment are presented in Fig. 9, which compares CO desorption from the Au substrate with CO desorption from a H_2O ice film. ^{13}CO was adsorbed on the ice film simply to ensure that N_2 did not contribute to the CO desorption trace. The mass spectrometer sensitivity toward ^{12}CO and ^{13}CO was assumed to be the same, and the yields of desorbed CO in the two experiments were identical within experimental error. CO desorbs from the Au substrate with multilayer and monolayer peaks, clearly evident at 29 and 32 K, respectively. This result compares favorably with those obtained in previous studies of single crystal metal surfaces.[29,30] However, in the desorption trace from the ice film, measured here for the first time, we believe small multilayer desorption is apparent at 29 K, with a broad, flat desorption peak with a maximum at roughly 50 K. A comparison of RAIR spectra of ^{12}CO deposited on amorphous ice with those of CO deposited on Au (not displayed here) shows minimal broadening of the CO stretching mode, indicating that CO is not adsorbed on multiple sites with varying adsorption energies. It is believed that the broad TPD peak results from diffusion of CO into the porous structure of the ice film, analogous to the behavior of N_2 adsorbed on amorphous ice.[31] Such diffusive behavior might be investigated experimentally by varying the temperature ramp and the thickness of the ice film, and modeled by including an equation for the diffusion process in chemical reaction simulations.[32]

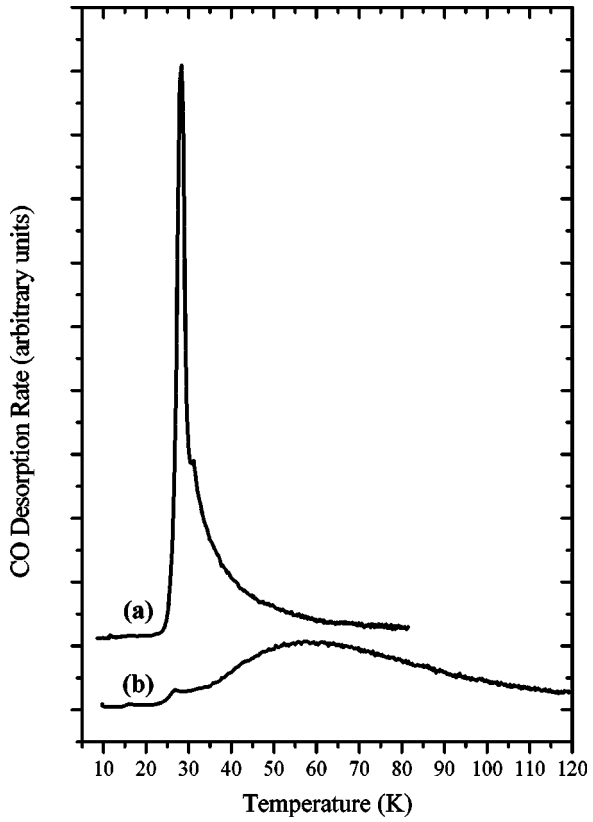

FIG. 9. TPD spectra of (a) a Au substrate at 10 K exposed to 20 L ^{12}CO and (b) a 0.04 μm H_2O-ice film at 10 K exposed to 20 L of ^{13}CO.

In the results described above, the adsorption conditions for the H_2O-ice film growth (10 K, 10^{-8} mbar) result in an amorphous, high-density (highly porous) film.[33] A number of previous experiments on H_2O-ice films by Kay and coworkers using molecular beam dosing have established that the morphology of the H_2O-ice layer is affected by the deposition conditions.[31] The surface temperature affects the ice phase obtained and the angle of incidence affects the ice porosity. In this system, at a surface temperature above 130 K cubic crystalline ice is formed, below this temperature amorphous ices with varying degrees of porosity are formed.[34] This experiment was designed with a quasidirective effusive molecular source to recreate as far as possible the conditions in the ISM, where deposition is essentially randomized, i.e., equally probable at all angles. The ice porosity can be partially controlled by rotating the sample relative to the position of the dosing source, and by changing the dosing temperatures and annealing times. For example, in H_2O ice, films without pores are produced at surface temperatures above 80 K. The film can then be cooled to 10 K, retaining its nonporous structure. At dosing temperatures between 80 and 20 K the degree of porosity increases; the most porous ices in this system are obtained at 6 K. Alternatively,

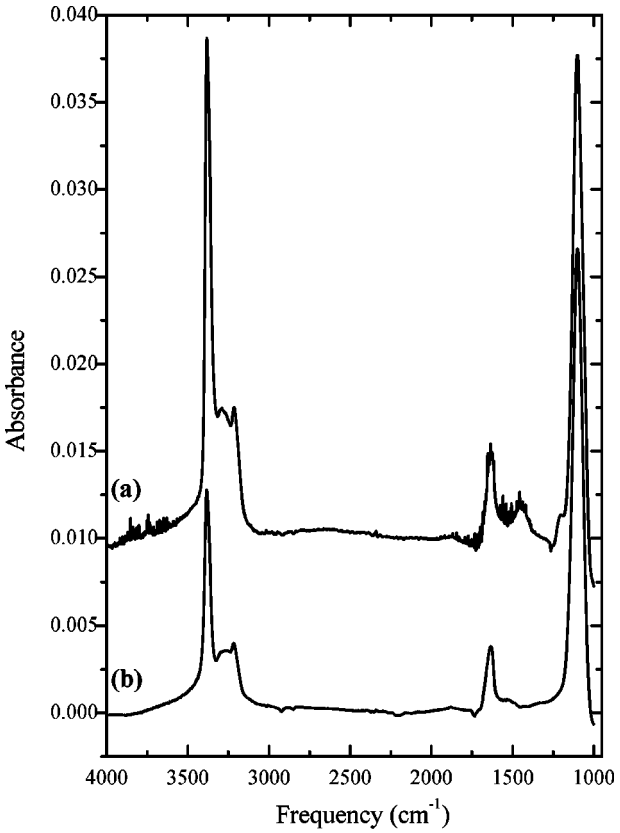

FIG. 10. RAIR spectra of ammonia films at 10 K: (a) 50 L exposure recorded at a grazing angle of 75° and (b) 200 L exposure recorded at a grazing angle of 84°.

it is possible to control the porosity of the H_2O-ice layer by dosing at 10 K, and then annealing the film at higher temperatures. Above 80 K the annealing process also leads to pore collapse, so by varying the annealing time it is possible to vary the pore concentration. The diffusion of other molecular species into and out of these porous pockets is an important concern. It is envisaged that other amorphous molecular solids exhibit similar porous behavior. In astronomical terms it could help to explain the outgassing rates of comets and trapping of complex molecular species in interstellar and planetary ices. One potential route for solid state chemical reactions in the ISM is for simple atomic and molecular species to diffuse into these porous pockets at low temperature, becoming trapped rather than desorbing as the ice warms up, and then diffusing through the ice with sufficient energy to overcome activation barriers, and reacting to form more complex molecular species such as CO_2 and CH_4. This apparatus can be exploited to study these interactions in detail, and is currently being used to study the interplay between CO, CO_2, H_2O, and NH_3 in a variety of bi- and trimolecular mixtures. Details of the CO–H_2O ice system are reported elsewhere.[35]

B. FT-RAIRS

Preliminary RAIR spectra of ammonia films were recorded at grazing angles of 75° and 84°, as displayed in Fig. 10. When the apparatus is configured for RAIRS at 75°, the sample faces the gas dosers. However, when configured for RAIRS at 84°, the sample faces away from the gas dosers, so that adsorption onto the sample occurs from the background pressure in the chamber during dosing. Therefore, the 50 L exposure in the 75° experiment [Fig. 10(a)] and the 200 L exposure in the 84° experiment [Fig. 10(b)] actually represent films of approximately equal thickness. The spectra show a general similarity to previously published infrared transmission spectra.[36] The peaks in Fig. 10(a) can be assigned, as indicated in Table I, by referring to published vibrational frequencies determined by high resolution electron energy-loss spectroscopy (HREELS) for ammonia adsorbed on a Ag(110) surface.[37]

TABLE I. Assigment of features in the RAIR spectrum of the NH_3 film, shown in Fig. 10(a). ν=stretch, δ=bend, a_1=totally symmetric, e_1=doubley degenerate, L=libration, R_{xy}=rotation about the axis in the x–y plane.

NH_3 film/ Au (cm^{-1})	Relative intensity	Vibrational mode	NH_3 gas phase fundamental (cm^{-1})[a]
1100	Very strong	δa_1 (HNH) "umbrella" bend	940
1200	Weak	$3\nu_L(R_{xy})$	
1450	Weak	$\nu_L(R_{xy})+\delta a_1$(HNH)	
1630	Medium	δe_1(HNH) "scissor" bend	1628
3160–3315	Medium	νa_1(NH)	3336
3380	Strong	νe_1(NH)	3414

[a]Reference 40.

There are several aspects of the spectrum recorded at 84° that are different from those in the 75° experiment. Spectral noise in the 1500–2000 and 3700–4000 cm^{-1} ranges is absent in the 84° experiment. These features result from gas phase H_2O absorption, indicating an incomplete purge of the optics boxes, and therefore can be ignored. However, the absence of the overtone and combination features, the slight change in the peak shape in the symmetric N–H stretch region, and the reduction of the relative intensity of the N–H stretch features are of real significance. Such changes result from variation of the underlying surface reflectivity, which is a function of both the wavelength and the angle of incidence of the infrared beam.

The optical properties of the film (the real and imaginary components, n and k, of the complex refractive index, $\tilde{n}$, can be calculated by applying the Fresnel equations[38] in a form appropriate for this type of system.[39] Using these properties, laboratory RAIR spectra may be manipulated to allow direct comparison with transmission infrared spectra of astronomical objects.

C. QCM

Figure 11 shows the H_2O uptake measured by the QCM. These data illustrate the sensitivity of the QCM as it operates under simultaneous low temperature and UHV conditions. In this type of measurement the QCM is employed an alternative (or more commonly an additional) source of data from which uptake curves can be measured. It is operated in isothermal mode, where it used to determine the mass of material deposited on the substrate. If the gas flow rate into the chamber during deposition is also known, then these data from the QCM can also be used to accurately determine

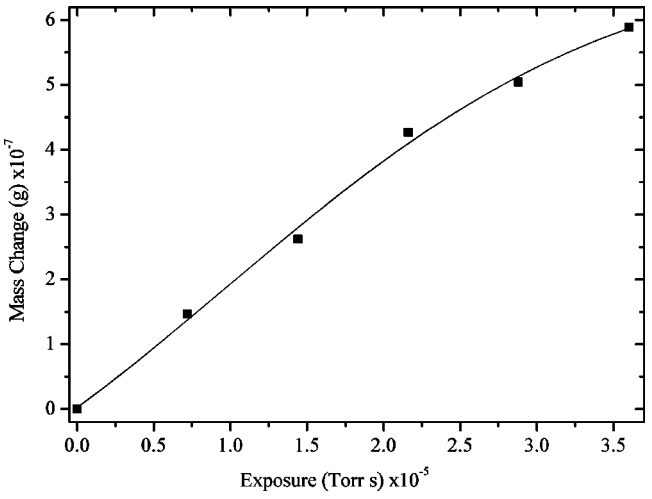

FIG. 11. Mass increase calculated from the change in the QCM difference frequency during exposure of the Au substrate on the quartz crystal to H_2O. The total change in mass is equivalent to 20 bilayers of adsorbed H_2O.

sticking coefficients between adsorbate gases and molecular ices over a range of temperatures that are significant in the ISM and young stellar objects (YSOs).

As a standalone instrument the QCM does not provide any additional information on sticking probabilities, coverage, or uptake that could not have been obtained by LoSMS and TPD measurements using the QMS. The initial experiments have focused on proving the functionality of such an instrument under the low temperature and low pressure conditions of this experiment. However, when combined with RAIRS and TPD measurements, isothermal QCM mass measurements will offer specific advantages for complex studies of film porosity and chemical reactivity. A combination of QCM mass measurements versus film thickness measurements (using a simple He–Ne laser interference pattern) can be used to estimate the density and, consequently, porosity of an ice layer. The ice is then dosed with a second species, which fills the pores. The uptake of this second species can be determined from the change in mass measured by the QCM. In combination with ice thickness measurements, these experiments allow us to explore the nature and behavior of the porous ices over a range of temperatures. Second, the QCM is useful in reactive etching measurements. If isothermal coadsorption of a number of atomic, radical, and molecular species leads to chemical reactions at the surface, or in the pores of the ice layer, some species are likely to desorb. A combination of RAIRS, TPD, and mass measurements will assist in tracing and elucidating the mechanisms involved in such complex processes. These systems are very representative of complex gas-grain chemistry that occurs in the cold regions of the ISM.

ACKNOWLEDGMENTS

The authors thank the Particle Physics and Astronomy Research Council (PPARC), School of Chemistry of the University of Nottingham, and the University of Nottingham Research Innovation Fund for their support of this research. The authors also wish to thank Neil Barnes and Dave Litchfield for their assistance during the construction of this experiment. General thanks go to those in glassblowing and mechanical workshop services at the School of Chemistry, University of Nottingham. Finally, thank you to Peter Ainsworth, Beatrice Aubrey, John Dever, and Timothy Weston for their experimental contributions to the work described in Secs. II and III.

[1] D. A. Williams, Faraday Discuss. **109**, 1 (1998).
[2] M. P. Bernstein, S. A. Sandford, and L. J. Allamandola, Sci. Am. **281**, 42 (1999).
[3] D. C. B. Whittet, in *Dust and Gas in Astronomy*, edited by T. J. Millar and D. A. Williams (Oxford University Press, Oxford, 1993), Chap. 2, p. 27.
[4] E. Herbst, in *IAU Symposium No. 197 Astrochemistry: From Molecular Clouds to Planetary Systems*, edited by Y. C. Minh and E. F. van Dishoeck (Astronomical Society of the Pacific, San Francisco, CA, 2000), Chap. 2, p. 147.
[5] D. P. Ruffle and E. Herbst, Mon. Not. R. Astron. Soc. **322**, 770 (2001).
[6] Y. Aikawa, T. Umebayashi, T. Nakanao, and S. M. Miyama, Astrophys. J. **519**, 705 (1999).
[7] C. Lu and A. W. Czanderna, *Applications of Piezo-electric Quartz Crystal Microbalances* (Elsevier, Amsterdam, 1994).
[8] G. Suaerbrey, Z. Phys. **155**, 206 (1959).
[9] J. D. Beckerle, Q. Y. Yang, A. D. Johnson, and S. T. Ceyer, Surf. Sci. **195**, 77 (1988).
[10] H. Schlichting and D. Menzel, Rev. Sci. Instrum. **64**, 2013 (1993).
[11] P. W. Atkins, *Physical Chemistry*, 5th ed. (Oxford University Press, Oxford, 1994), Chap. 6, p. 198.
[12] M. Stichler, P. Zebisch, M. Weinelt, and H. P. Steinruck, Surf. Sci. **348**, 370 (1996).
[13] Z. Dohnalek, G. A. Kimmel, S. A. Joyce, P. Ayotte, R. S. Smith, and B. D. Kay, J. Phys. Chem. B **105**, 3747 (2001).
[14] A. F. Carlsson and R. J. Madix, Surf. Sci. **487**, 201 (2001).
[15] A. Klekamp and E. Umbach, Surf. Sci. **284**, 291 (1993).
[16] A. F. Carlsson and R. J. Madix, J. Chem. Phys. **114**, 5304 (2001).
[17] A. F. Carlsson and R. J. Madix, Surf. Sci. **458**, 91 (2000).
[18] C. Ramseyer, C. Girardet, F. Bartolucci, G. Schmitz, R. Franchy, D. Teillet-Billy, and J. P. Gauyacq, Phys. Rev. B **58**, 4111 (1998).
[19] Y. P. Hyu, K. Jacobi, and H. H. Rotermund, Surf. Sci. **117**, 581 (1982).
[20] H. Schlichting and D. Menzel, Surf. Sci. **272**, 27 (1992).
[21] C. Backx, C. P. M. De Groot, and P. Biloen, Surf. Sci. **104**, 300 (1981).
[22] R. G. Jones and S. Turton, Surf. Sci. **377–379**, 719 (1997); R. G. Jones and C. J. Fisher, *ibid.* **424**, 127 (1999).
[23] D. P. Woodruff and T. A. Delchar, *Modern Techniques of Surface Science*, 2nd ed. (Cambridge University Press, Cambridge, 1994), Chap. 9, p. 532.
[24] P. Hollins, Vacuum **45**, 705 (1994).
[25] R. G. Greenler, J. Chem. Phys. **44**, 310 (1966).
[26] R. Helsel, *Visual Programming with HP-VEE*, 2nd ed. (Prentice–Hall, Englewood Cliffs, PTR, NJ, 1997).
[27] D. A. King, Surf. Sci. **47**, 384 (1975).
[28] A. Bar-Nunn, I. Kleinfeld, and E. Kochavi, Phys. Rev. B **38**, 7749 (1988).
[29] C. Ruggiero and P. Hollins, J. Chem. Soc., Faraday Trans. **92**, 4829 (1996).
[30] J. P. Camplin, J. C. Cook, and E. M. McCash, J. Chem. Soc., Faraday Trans. **91**, 3563 (1995).
[31] G. A. Kimmel, K. P. Stevenson, Z. Dohnálek, R. S. Smith, and B. D. Kay, J. Chem. Phys. **114**, 5284 (2001).
[32] G. Ellis, J. Sidaway, and M. R. S. McCoustra, J. Chem. Soc., Faraday Trans. **94**, 2633 (1998).
[33] P. Jenniskens, D. F. Blake, M. A. Wilson, and A. Pohorille, Astrophys. J. **455**, 389 (1995).
[34] H. J. Fraser, M. P. Collings, M. R. S. McCoustra, and D. A. Williams, Mon. Not. R. Astron. Soc. **327**, 1165 (2001).
[35] M. P. Collings, H. J. Fraser, J. W. Dever, and M. R. S. McCoustra, Astrophys. J. Lett. (in press).
[36] S. A. Sandford and L. J. Allamandola, Astrophys. J. **417**, 815 (1993).
[37] J. L. Gland, B. A. Sexton, and G. E. Mitchell, Surf. Sci. **115**, 623 (1982).
[38] O. S. Heavens, *Optical Properties of Thin Films* (Butterworths, London, 1955), p. 53.
[39] J. D. E. McIntyre and D. E. Aspnes, Surf. Sci. **24**, 417 (1971).
[40] G. Herzberg, *Molecular Spectra and Molecular Structure*, Vol. 2 Infrared and Raman Spectra of Polyatomic Molecules (Van Nostrand Reinhold, New York, 1945), p. 295.